FRA-75-1

REPORT NO FRA-ORD&D-75-40

EVALUATION OF LINEAR INDUCTION MOTOR CHARACTERISTICS: THE YAMAMURA MODEL

John J. Stickler

APRIL 1975
INTERIM REPORT

Prepared for
U.S. DEPARTMENT OF TRANSPORTATION
FEDERAL RAILROAD ADMINISTRATION
Office of Research, Development and Demonstrations
Washington DC 20590

TECHNICAL REPORT STANDARD TITLE PAGE

1. Report No.	2. Government Accession No.	3. Recipient's Catalog No.
FRA-ORD&D-75-40		

4. Title and Subtitle	5. Report Date
EVALUATION OF LINEAR INDUCTION MOTOR CHARACTERISTICS: THE YAMAMURA MODEL	April 1975
	6. Performing Organization Code DOT-TSC-FRA-75-1
7. Author(s) John J. Stickler	8. Performing Organization Report No.
9. Performing Organization Name and Address U.S. Department of Transportation Transportation Systems Center Kendall Square Cambridge MA 02142	10. Work Unit No. RR505/R5316
	11. Contract or Grant No.
12. Sponsoring Agency Name and Address U.S. Department of Transportation Federal Railroad Administration Office of Research, Development and Demonstrations Washington DC 20590	13. Type of Report and Period Covered Interim Report March - September 1974
	14. Sponsoring Agency Code
15. Supplementary Notes	

16. Abstract

The Yamamura theory of the double-sided linear induction motor excited by a constant current source is discussed in some detail. The report begins with a derivation of thrust and airgap power using the method of vector potentials and theorem of residues. The LIM thrust computed via the theorem of residues is compared with similar results obtained using numerical integration. Both methods are seen to yield equivalent results providing the increments in the numerical integration are made sufficiently small. The finite width and length of the primary alter the LIM thrust considerably in the regions of large and small slip frequencies respectively. The effect of finite primary dimensions on LIM thrust is discussed in detail for the examples of the TLRV & LIMRV LIM's operating at rated speeds. A comparison of thrusts predicted by the Yamamura, Oberretl, and Elliott LIM models for the TLRV & LIMRV motors show fair agreement in the value of thrusts predicted by the different theories.

17. Key Words	18. Distribution Statement
Linear Induction Motor LIM Propulsion Characteristics End-Effect Edge-Effect	DOCUMENT IS AVAILABLE TO THE PUBLIC THROUGH THE NATIONAL TECHNICAL INFORMATION SERVICE, SPRINGFIELD, VIRGINIA 22161

19. Security Classif. (of this report)	20. Security Classif. (of this page)	21. No. of Pages	22. Price
Unclassified	Unclassified	42	

Form DOT F 1700.7 (8-69)

PREFACE

This report discusses the Yamamura two-dimensional theory of linear induction motors and its application to the analysis of the high-speed propulsion characteristics of linear induction motors. It is the second in a three-part series devoted to a review of current LIM theories and the presentation of computer programs based on these theories. The first report, dealing with the Oberretl theory, and the final report, treating the Mosebach theory, discuss important aspects of idealized models used in the respective theories. The three reports taken together provide an interesting comparison of predicted motor characteristics and their relation to the models upon which they are based.

The author is pleased to acknowledge the following individuals for numerous discussions and helpful information: Mr. Matthew Guarino, Jr., of the U.S. Federal Railroad Administration, Dr. David G. Elliott of Jet Propulsion Laboratory, Dr. Clem Skalski of MITRE Corporation, and Professor James Melcher of the Massachusetts Institute of Technology.

TABLE OF CONTENTS

LIST OF ILLUSTRATIONS

LIST OF TABLES

1. INTRODUCTION

This report discusses the Yamamura theory of the linear induction motor (LIM) as presented in the text, "Theory of Linear Induction Motors" by S. Yamamura (University of Tokyo, Japan).[1] It represents the second in a series of reports dealing with current theories of linear induction motors and their application to computer analysis. The previous report, entitled "Evaluation of Linear Induction Motor Characteristics: The Oberretl Model" discussed the Oberretl theory of the linear induction motor as presented at the Symposium on Linear Motors, Capri, Italy, June 19-21, 1973. A third report dealing with the Mosebach (University of Braunschweig, Germany) remains to be published. The latter will comprise the final in this series of reports reviewing current theories of linear induction motors.

This report has three primary objectives. The first is to examine the Yamamura LIM model and the basic assumptions upon which it is derived. The second is to develop the computer software needed for numerical studies of LIMs based on the Yamamura model. The third is to apply the software technology to computer analyses of the TLRV and LIMRV LIM propulsion characteristics.

The Yamamura treatment of the linear induction motor differs from that of the others in several respects. It assumes the primary mmf to be describable by a single spatial harmonic and neglects the higher-order mmf harmonics resulting from the Fourier analysis of the actual winding current distribution of the LIM. The Yamamura approach uses the Fourier transform representation to describe the magnetic vector potential and evaluates the thrust using the theorem of residues.

The organization of the report is as follows. Section 2.1 discusses the Yamamura LIM model and its application to evaluating LIM thrust. Subsections 2.1.1 through 2.1.4 consider the residue theorem and the comparative thrusts obtained using the residue-versus-numerical integration techniques. Section 2.2 and subsequent

subsections discuss the Yamamura LIM theory with corrections for finite width of the motor. Section 3 summarizes the conclusions derived from the previous sections.

2. TECHNICAL DISCUSSION

2.1 THE YAMAMURA LIM MODEL AND MATHEMATICAL REPRESENTATION

The model for the two-dimensional analysis (neglecting edge-effects) is shown in Figure 1 with coordinate axes as indicated in the figure. The model is divided into three regions along the y-direction and into three zones along the x-direction. Region 1 is the iron core (primary), Region 2 is the secondary conductive sheet, and Region 3 is the air gap separating primary and secondary.

The assumptions appropriate to the Yamamura LIM model are:

1) The field is uniform in the z-direction and all variables are independent of z, i.e., $d(\ )/dz=0$.

2) The stator windings are approximated by sinusoidally traveling surface current sheets existing between x=0 and x=L of the stator core surface.

$$j_1 = J_1 \, e^{j(\omega t - kx)} \tag{1}$$

Winding slot perturbations and effect of three-phase stator current unbalance are ignored.

3) The stator core extends to infinity in both directions of x-coordinate and has permeability $\mu >> \mu_o$. Magnetic end-effects are neglected.

The Yamamura treatment considers spatial variations of current and flux density only along the x- and y-directions. Since primary current flows in the z-direction, $\overline{B}$ and $\overline{H}$ have x and y components but no z component. The formulation of the electrodynamic problem begins with Maxwell's equations using a flux density, $\overline{B}$, derived from the vector potential, $\overline{A}$,

$$\overline{B} = \nabla x \overline{A} \tag{2}$$

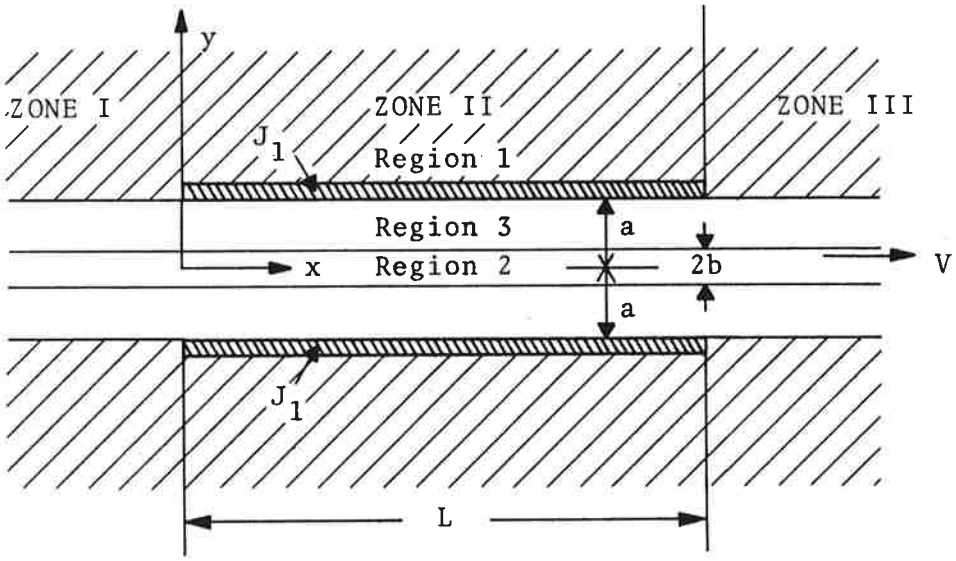

Figure 1. Yamamura Model for Two-Dimensional Analysis of a Linear Induction Motor

and

$$\nabla \cdot \bar{A} = 0$$

The general field equation expressed in terms of the vector potential then becomes,

$$\nabla^2 A_z = \mu\sigma\left(\frac{\alpha A_z}{\alpha t} + V\,\frac{\alpha A_z}{\alpha t}\right) \tag{3}$$

where $\bar{A}$ has only a z component. V is the velocity of the secondary relative to the fixed primary (stator), σ is the electrical conductivity of the rail, and μ its permeability.

The complete solution of the wave equation requires the boundary conditions to be satisfied at each interface of a given zone of the LIM model. Writing Maxwell's equations at the boundary of each region gives the following relations:

$$\frac{B_{1x}}{\mu_1} - \frac{B_{3x}}{\mu_3} = j_1 \qquad \frac{1}{\mu_1}\frac{dA_1}{dy} - \frac{1}{\mu_3}\frac{dA_3}{dy} = j_1 \text{ at } y = \pm a \text{ ZONE II} \tag{4}$$

where j_1 is the surface current density defined by Equation (1).

$$B_{1y} = B_{3y} \qquad \frac{dA_1}{dx} = \frac{dA_3}{dx} \qquad \text{at } y = \pm a \text{ ZONE II} \tag{5}$$

$$\frac{B_{3x}}{\mu_3} = \frac{B_{2x}}{\mu_2} \qquad \frac{1}{\mu_3}\frac{dA_3}{dy} = \frac{1}{\mu_2}\frac{dA_2}{dy} \qquad \text{at } y = \pm b \text{ ZONE II} \tag{6}$$

$$B_{3y} = B_{2y} \qquad \frac{dA_3}{dx} = \frac{dA_2}{dx} \qquad \text{at } y = \pm b \text{ ZONE II} \tag{7}$$

The solution for the vector potential in the airgap region (Region 3) is given by the Fourier transform.

$$A_3(x,y) = \frac{1}{2\pi}\int_{-\infty}^{\infty} \frac{\mu_o \tilde{J}_1\left[\cosh\gamma b\cosh\xi(y-b) + \frac{\gamma}{\xi}\sinh\gamma b\sinh\xi(y-b)\right]}{\xi\cosh\gamma b\sinh\xi(a-b) + \gamma\sinh\gamma b\cosh\xi(a-b)}\, e^{j\xi x} d\xi \tag{8}$$

where

$$\gamma^2 = \xi^2 + j V \mu_2 \sigma_2 \xi + j \omega \mu_2 \sigma_2$$

and $\tilde{J}_1$ is the transform of the primary current density.

$$\tilde{J}_1(\xi) = \int_{-\infty}^{\infty} J_1 e^{-jkx} e^{-j\xi x} dx$$

$$= j \frac{J_1 \left(e^{-j(\xi+k)L} - 1 \right)}{\xi + k} \tag{9}$$

The solution of the vector potential transform given by Equation (8) then leads to the LIM thrust and airgap power per unit width in the z direction.

$$F_x = \frac{-1}{2} \int_0^L \mathrm{Re} \left(j_1^*(x) \frac{dA_3}{dx}(x,a) \right) dx \tag{10}$$

$$P_{airgap} = \frac{-1}{2} \int_0^L \mathrm{Re} \left(j\omega A_3^*(x,a) \cdot j_1(x) \right) dx \tag{11}$$

A discussion of the use of theorem of residues to evaluate the vector potential transform is given in the next section.

2.1.1 Solution of Vector Potential Integral Using Residue Theorem

The residue theorem states that the integral of an analytic function around a closed contour is equal to the sum of the residues.[2] Thus if f(z) is an analytic function

$$\frac{1}{2\pi i} \int_{\substack{\text{closed} \\ \text{contour}}} f(z)\, dz = \sum \text{residues} \tag{12}$$

The solution for the residues directly follows once the poles of f(z) are found within the specified analytic region.

It is helpful to simplify the form of Equation (8) through the following substitutions:

$$G(\xi,y) = \cosh\gamma b\cosh\xi(y-b) + \frac{\mu_3\gamma}{\mu_2\xi}\sinh\gamma b\sinh\xi(y-b) \qquad (13)$$

$$H(\xi) = \xi\cosh\gamma b\,\sinh\xi(a-b) + \frac{\mu_3\gamma}{\mu_2}\sinh\gamma\cosh\xi(a-b) \qquad (14)$$

Then the airgap vector potential is given by

$$A_3(x,y) = \frac{j\mu_o}{2\pi}\int_{-\infty}^{\infty} J_1 e^{j\xi x}\quad\frac{e^{-j(\xi+k)L}-1}{\xi+k}\quad\frac{G(\xi,y)}{H(\xi)}\,d\xi \qquad (15)$$

where the poles of f(z) correspond to the roots of

$$(\xi + k)\,H(\xi) = 0 \qquad (16)$$

Equating the three principal roots of Equation (16) to ξ_1, ξ_2, and ξ_3, the residue theorem leads to the following relation for the vector potential in the airgap in Zone 2($0 < x < L$).

$$A_3(x,y) = \mu_o J_1\left[\frac{G(\xi_1,y)e^{j\xi_1 x}}{H(\xi_1)}\frac{}{} + \frac{G(\xi_2,y)e^{j\xi_2 x}}{(\xi_2+k)\left.\frac{dH}{d\xi}\right|_{\xi=\xi_2}}\right. \qquad (17)$$

$$\left. + \frac{G(\xi_3,y)e^{-j(\xi_3+k)L}e^{j\xi_3 x}}{(\xi_3+k)\left.\frac{dH}{d\xi}\right|_{\xi=\xi_3}}\right]$$

2.1.2 Solution of $H(\xi)=0$ via the Newton-Raphson Method[3]

The residues of the vector potential integral described by Equation (9) are found once the roots of Equation (16) have been determined. One root is simply $\xi_1=-k$. An infinite number of additional roots remain, however, corresponding to the solution of the transcendental equation $H(\xi) = 0$. Such an infinite number of roots is characteristic of wave solutions describing the propagation of waves within regions with multi-defined boundaries, as for example, the propagation of electromagnetic and sonic waves inside cylinderical waveguides. Yamamura points out (Ref. 1, p. 73) that only two of these infinite number of roots need to be considered in his mathematical treatment since the other roots lie far from the origin in wave number space and describe waves which are highly attenuated. The justification for this is later born out in the results of Section 2.1.4, in which the thrust evaluated by numerically integrating the "exact" thrust function (described by an infinite number of wave vector roots) is closely equal to the thrust found in the Yamamura method (in which only the dominant roots, ξ_1, ξ_2, ξ_3, are considered).

Yamamura suggests the application of the Newton-Raphson method for evaluating the roots ξ_2 and ξ_3. According to this method, starting with an initial approximation to the root, successive iterations are made leading to increasingly better approximations to the final root. Thus if ξ' represents the initial estimate of the root given by the thin sheet approximation, the Newton-Raphson method states that the new approximation to the root is obtained by repeated iterations of

$$\xi = \xi' - \frac{H(\xi)}{\left.\frac{dH(\xi)}{d\xi}\right|_{\xi=\xi'}} \tag{18}$$

Tables 1 and 2 give the roots computed for the TLRV and LIMRV LIMs according to Newton-Raphson method using the motor parameters shown below:

TABLE 1. ROOTS OF $H(\xi) = 0$ FOR TLRV LIM; EDGE-EFFECTS NEGLECTED. LIM SPEED = 300 MPH

Freq. Hz	ξ_1	ξ_2	ξ_3
150	-7.012	-7.02+j0.07	0.21-j262.04
155	-7.012	-7.26+j0.08	0.21-j262.04
160	-7.012	-7.49+j0.08	0.22-j262.04
165	-7.012	-7.73+j0.09	0.23-j262.04
170	-7.012	-7.96+j0.10	0.23-j262.04
175	-7.012	-8.20+j0.10	0.24-j262.04
180	-7.012	-8.43+j0.11	0.25-j262.04
185	-7.012	-8.66+j0.11	0.25-j262.04
190	-7.012	-8.90+j0.12	0.26-j262.04
195	-7.012	-9.13+j0.13	0.27-j262.04
200	-7.012	-9.37+j0.13	0.27-j262.04

TABLE 2. ROOTS OF $H(\xi) = 0$ FOR LIMRV LIM; EDGE-EFFECTS NEGLECTED. LIM SPEED = 250 MPH

Freq. Hz	ξ_1	ξ_2	ξ_3
160	-8.840	-8.99+j0.19	0.25-j186.39
165	-8.840	-9.27+j0.20	0.26-j186.39
170	-8.840	-9.55+j0.21	0.27-j186.39
175	-8.840	-9.83+j0.22	0.27-j186.39
180	-8.840	-10.11+j0.23	0.28-j186.39
185	-8.840	-10.39+j0.25	0.29-j186.39
190	-8.840	-10.67+j0.26	0.30-j186.39
195	-8.840	-10.95+j0.27	0.30-j186.39
200	-8.840	-11.23+j0.29	0.31-j186.39

TLRV LIM Parameters

Turns per Coil	(N)	=	4
Pole Pitch	(τ_p)	=	0.448 m.
Core Width	(2c)	=	0.1905 m.
Poles	(P)	=	5
Core Length	(ℓ_s)	=	2.56 m.
Air Gap	(g)	=	0.0171 m.
Phases	(m)	=	3
Slots per Phase	(q)	=	5
End Half-filled Slots	(ε)	=	5
Secondary Thickness	(b)	=	.0066 m.
Secondary Resistivity	(ρ)	=	$.416 \times 10^{-7}$ ohm-m.

LIMRV LIM Parameters

Turns per Coil	(N)	=	1
Pole Pitch	(τ_p)	=	.355 m.
Core Width	(2c)	=	.254 m.
Poles	(P)	=	10
Core Length	(ℓ_s)	=	3.81 m.
Air Gap	(g)	=	.024 m.
Phases	(m)	=	3
Slots per Phase	(q)	=	5
End Half-filled Slots	(ε)	=	5
Secondary Thickness	(b)	=	.0071 m.
Secondary Resistivity	(ρ)	=	0.416×10^{-7} ohm-m.

These roots describe the propagation constants of the three principal waves in Zone II. (See Figure 1.) ξ_1 corresponds to the propagation number of the 'driving'wave, ξ_2 the propagation number of the entrance end-effect wave, and ξ_3 the propagation number of the exit end-effect wave. The large imaginery part of ξ_3 indicates that the exit end-effect is highly damped for both LIM examples. It should, therefore, contribute little to the total LIM thrust.

2.1.3 Calculation of Thrust Residues (Edge-Effects Neglected)

The LIM thrust in the Yamamura model is found by substituting Equation (8) in Equation (10) and performing the required integration over the length of the motor. The solution obtained by

Yamamura for the time-average thrust is given in terms of three thrust residue functions, F_1, F_2, F_3.

$$F_x = F_1 + F_2 + F_3$$

where

$$F_1 = \frac{\mu_o}{2} J_1^2 \, \mathrm{Re}\left[\frac{jkLG(-k,a)}{H(-k)}\right] \tag{19}$$

$$F_2 = \frac{\mu_o}{2} J_1^2 \, \mathrm{Re}\left[\xi_2 \frac{\left(1-e^{j(\xi_2+k)L}\right)}{(\xi_1+k)^2 dH/d\xi_{\xi=\xi_2}} G(\xi_2,a)\right] \tag{20}$$

$$F_3 = \frac{\mu_o}{2} J_1^2 \, \mathrm{Re}\left[\xi_3 \frac{e^{-j(\xi_3+k)L}\left(1-e^{j(\xi_3+K)L}\right)}{(\xi_3+k)^2 dH/d\xi_{\xi=\xi_3}} G(\xi_3,a)\right] \tag{21}$$

The three thrust components, F_1, F_2, F_3 describe the thrusts developed by the normal wave, the entrance end-effect wave, and the exit end-effect wave.

The values of these thrust components were computed for the examples of the TLRV and LIMRV LIM's as described by the motor parameters previously given. The computed thrust components for these two motors are presented in Tables 3 and 4 as a function of motor excitation frequency. The tables demonstrate the relatively small magnitude of the exit end-effect thrust component compared to the entrance end-effect thrust component. The magnitude of F_2 increases sharply with decreasing slip frequency and approaches the magnitude of F_1 at zero slip frequency. The data in Table 4 also illustrates the oscillatory-like characteristics of F_2 as a function of slip frequency. The study of thrust residues will be continued in Section 2.2.1 where the effect of finite LIM width on thrust will be examined.

TABLE 3. COMPUTED THRUST "RESIDUES" FOR TLRV LIM; EDGE-EFFECTS NEGLECTED. LIM SPEED = 300 MPH

Freq. Hz	F_1 N.	F_2 N.	F_3 N.	F_x N.
150	9380	-9750	2.74	- 360
155	14100	-13800	2.74	343
160	7730	-6720	2.74	1020
165	5270	-3670	2.74	1600
170	3990	-1930	2.74	2060
175	3210	- 845	2.74	2370
180	2680	- 179	2.74	2510
185	2310	186	2.74	2490
190	2020	333	2.74	2360
195	1800	329	2.74	2130
200	1620	238	2.74	1860

TABLE 4. COMPUTED THRUST "RESIDUES" FOR LIMRV LIM; EDGE-EFFECTS NEGLECTED. LIM SPEED = 250 MPH

Freq. Hz	F_1 N.	F_2 N.	F_3 N.	F_x N.
160	15700	-14500	2.6	1210
165	11100	-7810	2.6	3320
170	7450	-2860	2.6	4590
175	5510	- 619	2.61	4890
180	4360	+ 98.8	2.61	4460
185	3590	+ 81.6	2.61	3680
190	3060	- 120	2.61	2940
195	2660	- 218	2.61	2440
200	2350	- 165	2.61	2190

2.1.4 Thrust Calculation: Theorem of Residues-Versus-Numerical Integration Methods

Yamamura applies the theorem of residues to evaluate the magnetic vector potential and subsequently the thrust based on Equation (10). A similar approach is adopted by Iwamoto[4] to compute LIM thrust. However, instead of applying the theorem of residues to evaluate the vector potential integral, he uses a numerical integration approach since it is claimed that the latter approach leads to a "more accurate analysis of the end-effect." This section will examine the two mathematical methods in terms of their computed LIM thrusts.

The Iwamoto expression for the thrust given by Equation (16) of Reference 4 is equivalent to the Yamamura expression for thrust as found by substituting Equation (8) in (10) and replacing the current density with its Fourier transform as given by Equation (9). (Note that the Yamamura thrust is computed for one core side only while the Iwamoto thrust is for both LIM sides.) The Yamamura expression for thrust can be rewritten as

$$F_x = \frac{\mu_o J_1^2}{4\pi} \int_{-\infty}^{\infty} 4\ \mathrm{Re}\left[j \left(\frac{\sin(\xi+k)L}{\xi + k} \right)^2 \frac{\xi G(\xi,a)}{H(\xi)} \right] d\xi \text{ per side} \qquad (22)$$

where $j = \sqrt{-1}$. The integral can be converted to a series format by replacing the variable wave number, ξ, by ν times the wave number increment, $2\pi/\ell$, where ℓ is a periodic length of a "unit cell" forming the basis for the fundamental wave number. Equation (22) then takes the form.

$$F_x = \frac{\mu_o J_1^2}{2\ell} \sum_{\nu} 4 \left(\frac{\sin \frac{L}{2}\left(\frac{\nu 2\pi}{\ell} + k \right)}{\frac{\nu 2\pi}{\ell} + k} \right)^2 \mathrm{Re}\left(j\xi \frac{G(\nu)}{H(\nu)} \right) \qquad (23)$$

where ν is summed over $-\infty$ to $+\infty$. The effect of finite primary width is not included in the above equation in its present form.

A comparative study was next undertaken to examine the possible variations in the thrust which result from the application

of the theorem of residues and numerical integration to evaluate the thrust integral. There is the question of the possible errors in the Yamamura thrust, which result from the neglect of the additional residues omitted in the evaluation of the vector potential integral. These additional residues neglected by Yamamura are associated with the multiple poles of $G(\xi,a)/H(\xi)$ which arise from the roots of $H(\xi)$ not located near the origin of the complex plane. A second question relates to possible inaccuracies in the numerical integration method resulting from the integration of the thrust distribution function in the region of the singularity.

Table 5 presents the thrusts computed by the residue method (Yamamura) and the numerical integration method (Iwamoto) for the example of the TLRV LIM operating at 300 mph. The value of the primary current density used in the residue thrust calculation was determined from

$$J_1 = \frac{6\sqrt{2}\,NI_1}{\tau_p}\,\frac{\sin q\alpha/2}{\sin\alpha/2}\,\sin\frac{\alpha'\pi}{2} \qquad (24)$$

where τ_p is the slot pitch and α' is the pitch factor equal to 2/3. The remaining parameters associated with the TLRV LIM are given in Table 1. The expression for the primary current density distribution used the numerical integration method is given by

$$J_1(\nu) = \frac{16NI\sqrt{2}\,m}{\pi\ell}\,\frac{\sin\nu q\alpha/2}{\sin\nu\alpha/2}\cdot\frac{\sin P\left(\frac{\nu mq\alpha-\pi}{2}\right)}{2\sin\left(\frac{\nu mq\alpha-\pi}{2}\right)}\cdot\sin\frac{\alpha'\pi}{2} \qquad (25)$$

The slot pitch for this case is equal to

$$\alpha = \frac{\text{motor length}}{\ell}\cdot\frac{2\pi}{85} \qquad (26)$$

Two separate sets of thrust calculations were made for the numerical integration method to study the effect of the size of the wave vector increment on the thrust result. The numerical summations were made over a range considered sufficient to encompass the main spectrum of the thrust distribution function. The numbers in

TABLE 5. COMPARATIVE TLRV LIM THRUSTS COMPUTED BY THEOREM OF RESIDUES AND NUMERICAL INTEGRATION METHODS

Freq. Hz	Residue Method[a] (Yamamura) N.	Numerical Integration[b] (Iwamoto) N. *	**
155	343	784(129)	347 (1)
160	1020	714(-30)	1011 (-1)
165	1600	1484(-7)	1597 (0)
170	2060	2241(9)	2063 (0)
175	2370	2255(-5)	2379 (0)
180	2510	2464(-2)	2536 (1)
185	2490	2554(2)	2541 (2)
190	2360	2362(0)	2418 (2)
195	2130	2146(1)	2202 (3)
200	1860	1885(1)	1935 (4)

(a) computed with J_1 defined by Equation (19)

(b) computed with $J_1(\nu)$ defined by Equation (20)

* periodic length ℓ = 33.212m.

** periodic length ℓ = 132.848m.

LIM speed = 300 MPH

parentheses specify the percent deviation in the thrust computed by the two methods. A glance at the table shows that the agreement is excellent between the residue method and the numerical summation method for the choice of a unit cell length equal to 132.848m. and reasonably good for the choice of a unit cell length equal to 33.212m. The results substantiate the equivalence of the two methods but point up the importance of the proper choice of wave number increment when numerically summing the thrust.

The expression for current density given by Equation (27) neglects the high-order harmonics associated with the number of slots per phase belt and number of phase belts per pole. A more complete description of the harmonic current density spectrum is given by the expression,

$$J(\nu) = \frac{16NI\sqrt{2}}{\pi \ell} \frac{\sin P\left(\frac{\nu mq\alpha - \pi}{2}\right)}{2 \sin\left(\frac{\nu qm\alpha - \pi}{2}\right)} \cdot \frac{\sin \nu q\alpha/2}{\sin \nu\alpha/2} \cdot \frac{\sin m\left(\frac{\nu q\alpha - \pi/m}{2}\right)}{\sin\left(\frac{\nu q\alpha - \pi/m}{2}\right)}$$

$$\cdot \sin\frac{\nu\alpha}{2} (mq - \varepsilon) \qquad (27)$$

where m is the number phases, and ε is the number of half-filled slots in the winding end turns. Table 6 presents the thrusts computed using Equations (25) and (27) for the example of the TLRV LIM. The value of periodic length was ℓ = 132.848 m. for both sets of calculations. The data shows that the use of the more complete current density expression given by Equation (27) results in significantly lower thrust values at low slip frequencies.

Several conclusions can be drawn from the thrust calculations presented in this section. The residue method and the numerical integration method yield equivalent results if the integration interval is made sufficiently narrow and the current densities used for both methods are consistent. Errors which result from the use of integration intervals which are too large tend to be more pronounced at low slip frequencies. When higher-order harmonics are included in the current density distribution function,

TABLE 6. COMPARATIVE TLRV LIM THRUSTS COMPUTED USING $J_1(\nu)$ DEFINED BY EQUATIONS (25) and (27). LIM SPEED = 300 MPH

Freq. Hz	F_x (J_1: Eqn 20) N.	F_x (J_1: Eqn 22) N.
155	347	-49.3
160	1011	696
165	1597	1384
170	2063	1957
175	2379	2368
180	2536	2597
185	2541	2644
190	2418	2535
195	2202	2313
200	1935	2027

the thrust is reduced at low slip frequencies. An advantage in utilizing the numerical integration technique is the comparative ease with which arbitrary winding current configurations can be included in the summation process.

2.2 THE YAMAMURA MODEL WITH EDGE-EFFECT CORRECTION

The previous discussion of the Yamamura LIM model considered the restrictive case when edge-effects (due to finite current sheet width) are assumed absent and the primary and secondary are infinitely wide. The computed thrusts describe the effect of a finite primary length on the total developed thrust of the LIM without regard to the effect of a finite primary width. When the finite width of the LIM is included in the analysis, the value of computed thrust is considerably altered. A study of linear induction motors with finite width primary and secondary structures by Bolton outlines one method for incorporating into the mathematical treatment the necessary corrections for edge-effects. The Bolton method consists of deriving a set of equivalent LIM parameters which are used to describe the effective secondary resistivity and magnetizing reactance of the LIM when edge currents are present. The parameters are derived by Bolton under the assumption that end-effects are absent and that the flux density immediately beyond the stator edges is zero. While the above assumptions are only approximately realized in practice, numerical studies based on the Bolton analysis have yielded satisfactory results in terms of actual-versus-computed flux density in the LIM air gap. The use of the Bolton method, therefore, represents a reasonable first-approximation approach to the edge-effect LIM correction.

2.2.1 The Bolton Correction for Finite LIM Width

The finite width of the primary is taken into account in the Yamamura analysis by utilizing the Bolton Theory[5] of linear induction motors for symmetrically positioned secondaries. The Yamamura model corrects for edge-effects by introducing an effective goodness factor and secondary current into the calculations. The latter factors were derived to maintain the same average airgap

flux density with edge currents as that determined in the absence of edge current and using the unmodified goodness factor and secondary current. In the presence of edge-effect, the effective goodness factor becomes,

$$G' = (K_R/K_X)\ G \tag{28}$$

where $G = \omega\mu_o\sigma b/aK^2$

The effective current density, J_1', likewise becomes,

$$J_1' = K_1\ J_1 \tag{29}$$

where

$$K_R = 1 - \mathrm{Re}\left\{(1-jsG)\ \frac{\lambda}{\alpha a}\ \tanh\alpha a\right\} \tag{30}$$

$$K_X = 1 + \mathrm{Re}\left\{(Gs+j)\ Gs\ \frac{\lambda}{\alpha a}\ \tanh\alpha a\right\} \tag{31}$$

$$K_1 = K_X\ \frac{1 + s^2G^2K_R^2/K_X^2}{1 + s^2G^2} \tag{32}$$

Yamamura ascribes to the secondary conductivity the same edge-effect dependence as that assigned to the goodness factor via Equation (28). This is only valid if the magnetizing reactance is held fixed and leads to some confusion when comparing equivalent parameters with those of Bolton.

LIM thrust including edge-effects is found by summing Equations 19-21, using the effective goodness factor G' in place of G, and the effective current density J_1' instead of J_1. Care must be exercised in substituting J_1' for J_1 since this substitution is made to "correct" the flux density at the primary resulting from the edge-effect perturbation. The primary current density remains constant in the Yamamura model as given by Equation 1. The correction for edge-effects requires that J_1^2 in Equations 19-21 be replaced with $J_1 \cdot J_1'$ and not $J_1'^2$.

The parameters K_1 and K_R/K_X were computed for the examples of the TLRV and LIMRV LIM's operating at the respective speeds of 300 and 250 mph. Tables 7 and 8 list the values of these parameters as a function of driving frequency. The effective secondary conductivities of both LIM's are reduced by a factor of at least two; the effective current densities also exhibit a pronounced decrease with increasing slip frequency.

2.2.2 Solution of $H(\xi)=0$ Via the Newton-Raphson Method; Edge-Effect Included

The solution of Equation (14) when the edge-effect is included in the treatment will be presented for completeness. The procedure described in Section 2.1.2 for determining the roots via the Newton-Raphson method was applied to the present calculations. Some difficulty was experienced in applying this method to the example of the TLRV LIM at higher slip frequencies, a situation not occurring in the previous calculation presented in Tables 3 and 4. When an attempt was made to determine ξ_3 using as an initial approximation of root of Equation (14) for small secondary thickness and airgap distance, the root determined by the Newton-Raphson method converged to ξ_2. The computer program was subsequently modified so as to set the initial approximation of ξ_3 equal to the value of the previous computed root determined at a somewhat different driving frequency. No difficulty was subsequently experienced in evaluating the roots of $H(\xi)$ after this modification.

The computed roots are presented in Tables 9 and 10 for the examples of the TLRV and LIMRV LIMs using the Bolton parameters given in Tables 7 and 8. For both motors, the imaginary part of ξ_3 is large, indicating that the corresponding "exit" end-effect waves are highly damped. The relative effect of the finite LIM width on ξ_2 can be seen by comparing the corresponding roots given in Tables 1 and 9 for the TLRV LIM and those given in Tables 2 and 10 for the LIMRV LIM. The tables show that the main effect of finite stator width is to increase the imaginary part of ξ_2 resulting in increased damping of the entrance end-effect wave. This is expected on a physical basis since edge-effects produce a constriction of

TABLE 7. BOLTON PARAMETERS COMPUTED FOR TLRV LIM.
MOTOR SPEED = 300 MPH

Freq. Hz	$\frac{K_R}{K_X}$	K_1
150	.40	1.0
155	.40	.99
160	.38	.95
165	.37	.91
170	.35	.87
175	.33	.83
180	.31	.79
185	.30	.76
190	.29	.73
195	.28	.71
200	.27	.69

TABLE 8. BOLTON PARAMETERS COMPUTED FOR LIMRV LIM.
MOTOR SPEED = 250 MPH

Freq. Hz	$\frac{K_R}{K_X}$	K_1
160	.57	.99
165	.55	.96
170	.52	.91
175	.49	.87
180	.46	.83
185	.44	.80
190	.42	.77
195	.41	.75
200	.39	.79

TABLE 9. ROOTS OF $H(\xi)=0$ FOR TLRV LIM; EDGE-EFFECTS INCLUDED. LIM SPEED = 300 MPH

Freq. Hz	ξ_1	ξ_2	ξ_3
150	-7.012	-7.02+j0.18	0.40-j252.63
155	"	-7.25+j0.20	0.42-j252.40
160	"	-7.48+j0.22	0.44-j251.86
165	"	-7.71+j0.25	0.48-j251.11
170	"	-7.94+j0.27	0.52-j250.27
175	"	-8.17+j0.31	0.56-j249.40
180	"	-8.40+j0.34	0.60-j248.55
185	"	-8.63+j0.37	0.65-j247.74
190	"	-8.86+j0.41	0.69-j246.98
195	"	-9.09+j0.45	0.74-j246.29
200	"	-9.32+j0.48	0.78-j245.64

TABLE 10. ROOTS OF $H(\xi)=0$ FOR LIMRV LIM; EDGE-EFFECTS INCLUDED. LIM SPEED = 250 MPH

Freq. Hz	ξ_1	ξ_2	ξ_3
150	-8.840	-8.41+j0.29	0.36-j182.64
155	"	-8.69+j0.30	0.37-j182.84
160	"	-8.97+j0.32	0.38-j182.83
165	"	-9.25+j0.35	0.40-j182.65
170	"	-9.53+j0.39	0.43-j182.35
175	"	-9.80+j0.43	0.46-j182.00
180	"	-10.08+j0.47	0.49-j184.64
185	"	-10.35+j0.52	0.52-j181.29
190	"	-10.63+j0.56	0.55-j180.96
195	"	-10.90+j0.61	0.58-j180.65
200	"	-11.17+j0.66	0.61-j180.37

secondary current flow near the stator edges and an increase in the secondary resistance; this results in more rapid attenuation in the end-effect wave distance.

2.2.3 Yamamura LIM Thrust with Edge-Effects Included

The thrust was next computed for the LIM models based on the TLRV and LIMRV LIM's and including the corrections for the finite width of the primary. Tables 11 and 12 give the magnitudes of the thrust components, F_1(normal wave), F_2(entrance end-effect wave), F_3(exit end-effect wave) for the TLRV and LIMRV LIM's driven at different line frequencies. The F_3 thrust component is negligibly small compared with F_1 and F_2 and can be discarded with little error in the final thrust result. This leads to an appreciable reduction in computer time, since it eliminates the lengthy calculation of one of the two roots of $H(\xi) = 0$.

A comparison of the thrusts computed by the Yamamura, Oberretl, and Elliott[6,7] models is given in Figures 2 and 3 for the TLRV and LIMRV LIM's. The Yamamura model gives consistently larger thrusts than the Elliott model. At peak thrust, the Yamamura thrust was 15 percent larger than the Elliott thrust for the LIMRV LIM and about 22 percent larger than the Elliott thrust for the TLRV LIM. The Yamamura model gave thrusts which correlated better with the Oberretl model than with the Elliott model, particularly for the TLRV LIM. It is interesting that for the TLRV LIM, the Yamamura and Oberretl models gave identical results at frequencies below 170 Hz.

It is worthwhile to review certain aspects of the different LIM models in the light of the results previously presented. The Yamamura model considers the fundamental mmf harmonic only and neglects higher-order mmf components. The inclusion of higher-order mmf harmonics in the Yamamura calculation would likely result in some reduction in computed thrust due to the negatively propagating 5-th harmonic wave; it is unlikely, however, that the thrust reduction would be sufficient to bring the Yamamura thrust into agreement with the Elliott result. Both Yamamura and Elliott

TABLE 11. PREDICTED THRUST FOR TLRV LIM USING YAMAMURA THEORY WITH EDGE-EFFECTS INCLUDED. MOTOR SPEED = 300 MPH

Freq. Hz	F_1 N.	F_2 N.	F_3 N.	F_x N.
150	3910	-4460	2.90	-548
155	24300	-23300	2.87	987
160	16900	-14500	2.78	2420
165	12300	-8670	2.67	3620
170	9570	-5050	2.56	4520
175	7830	-2750	2.46	5080
180	6620	-1310	2.36	5310
185	5740	- 476	2.28	5270
190	5070	- 58.8	2.21	5010
195	4540	86.4	2.15	4630
200	4110	73.9	2.10	4190

TABLE 12. PREDICTED THRUST FOR LIMRV LIM USING YAMAMURA THEORY WITH EDGE-EFFECTS INCLUDED. MOTOR SPEED = 250 MPH

Freq. Hz	F_1 N.	F_2 N.	F_3 N.	F_x N.
160	12700	-10800	2.68	1910
165	14800	-10000	2.63	4770
170	11500	-5010	2.56	6470
175	9000	-2070	2.47	6940
180	7340	- 804	2.39	6540
185	6180	- 431	2.32	5750
190	5340	- 378	2.26	4960
195	4690	- 356	2.20	4340
200	4190	- 286	2.15	3906

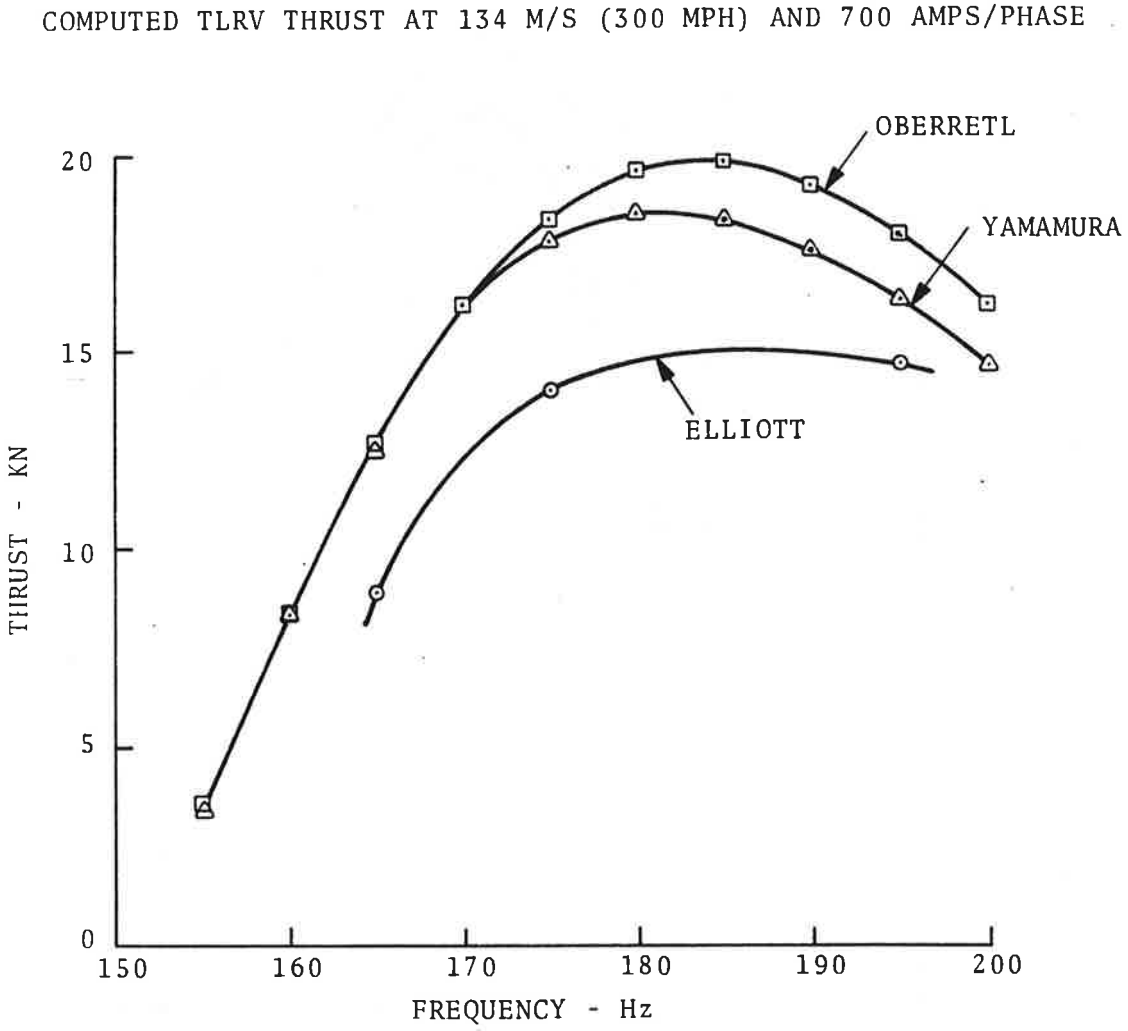

Figure 2. Computer Thrust Predictions for the TLRV LIM

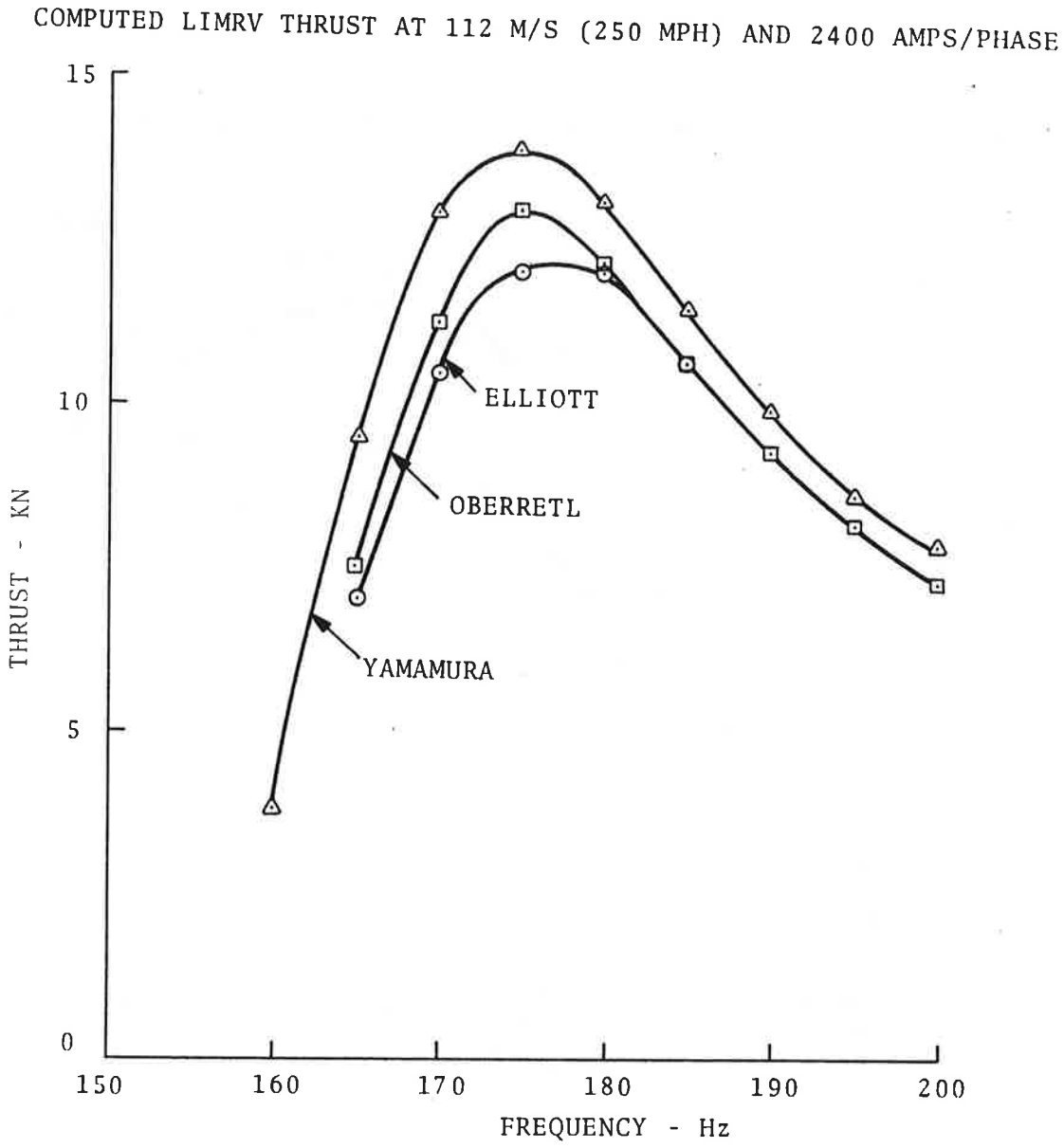

Figure 3. Computer Thrust Predictions for the LIMRV LIM

models compensate for edge-effects by modifying the values of the secondary resistivity and magnetizing reactance according to the method of Bolton. In deriving the appropriate factors to modify the secondary resistivity and magnetizing reactance, Bolton neglects end-effects. A glance at Tables 11 and 12 shows that end-effects have a dominant effect at low slip frequencies and could not be neglected when computing thrust. The possible error introduced into the result by neglecting end-effects in calculating Bolton factors and ultimately thrust remains unknown.

The Yamamura model described in this report uses the same value of secondary resistivity for both normal and end-effect secondary current waves. The constricted current flow pattern of the normal wave understandably results in an increased value of secondary resistivity. However, it is questionable whether the same current flow constriction exists for the end-effect current wave and whether its effective resistivity should be the same as that of the normal wave. The Oberretl treatment avoids the above complication by describing the current distribution as a multiple-harmonic Fourier representation and the secondary resistivity as the actual secondary resistivity.

Both the Yamamura and Oberretl LIM models assume a continuous primary ferromagnetic region and neglect the magnetic end-effect associated with the ferromagnetic boundaries. Yamamura argues that this assumption introduces little error into the calculation of LIM performance since the boundary conditions at the entrance end of the motor are very little affected by the highly damped exit end-effect wave. The Yamamura method then should give the correct normal and entrance end-effect waves and the LIM thrust, which is almost entirely determined by these waves, should be reasonably evaluated by this method. If the above condition is true, then one must look for other reasons to explain the discrepancies between the Yamamura and Elliott results. Part of the discrepancy can be traced to the neglect of higher-order mmf components in the Yamamura analysis and the use of a single harmonic wave to describe the LIM spatial winding current distribution. A more detailed study of the Yamamura-Elliott computer

models would be required, together with a correlation study of computed-versus-measured airgap flux densities, in order to explain the discrepancies between the predictions of the two theories.

3. CONCLUSIONS

The Yamamura analysis of the linear induction motor has been examined and a computer study of two high speed LIM's has been undertaken, based on the Yamamura LIM model. The results of the study indicate that the Yamamura theory predicts LIM thrusts in "reasonable" agreement with the corresponding predictions of the Oberretl and Elliott computer models. The Yamamura LIM thrusts tend to agree more closely with the Oberretl predictions than with those of Elliott. The divergence of the Yamamura and Elliott computed thrusts lies in the range of 15-30 percent for the two LIM examples considered.

The possible reasons for the predicted thrust discrepancies have been considered. The Yamamura model describes the primary mmf by a single spatial harmonic and neglects the effect of the higher-order mmf components. A computer study of the effect of these additional harmonics indicates that, for the example of the TLRV LIM, the additional mmf harmonics reduce LIM thrust considerably in the region of zero slip frequency and have a small effect on LIM thrust at higher slip frequencies. In the Yamamura model, edge-effects (current) are compensated by modifying the values of secondary resistivity and magnetizing reactance according to the theory by Bolton. The ultimate effect on LIM thrust of neglecting end-effects in the derivation of the Bolton factor is questionable, as is the effect of using a common value of effective secondary resistivity for both normal and end-effect secondary current waves.

The Yamamura LIM model assumes a continuous primary ferromagnetic region and neglects the magnetic end-effects associated with the ferromagnetic boundaries. Yamamura states that the above assumption results in negligible error in the LIM output characteristics, since the important boundary conditions at the entrance end of the motor are little affected by the highly damped exit end-effect wave. If the above condition is correct, then other explanations must be found to account for the discrepancies between

the Yamamura results and those of Elliott, based on a finite primary iron model.

The computer time required to run the Yamamura computer program is comparable with that required to run the Oberretl computer program, namely about 40-60 seconds for 10 case runs. This is approximately an order of magnitude less than the time required to run the same number of cases using the Elliott computer program.

REFERENCES

1. Yamamura S., Theory of Linear Induction Motors, Univ. Tokyo Press, 1972.

2. Ahlfors, L.V., Complex Analysis, McGraw-Hill, New York, 1966, p. 147.

3. Hartree, D.R., Numerical Analysis, Oxford Univ. Press, London, England, 1958, p. 214.

4. Iwamoto, M., Ohno, E., Itoh, T., and Shinryo, Y., "End-Effect of High Speed Linear Induction Motor," IEEE Trans. Ind. Appl., IA-9, (6), 632-639 (Nov./Dec. 1973).

5. Bolton, H., "Transverse Edge-Effect in Sheet-Rotor Induction Motors," Proc. IEE, 116, (5), 725-731 (May 1969).

6. Elliott, D., Ltr. to M. Guarino, DOT/FRA, May 29, 1973.

7. Elliott, D., Ltr. to M. Guarino, DOT/FRA, March 29, 1974.

APPENDIX

Summary of Computer Parameters and Equivalent Yamamura Parameters. (Ref.1, pp. 157-159)

Computer Parameters	Equivalent Yamamura Parameter	
AI1	I_1	Primary current amplitude
AJZ	$J_1 \cdot 10^5$	Primary current density $\cdot 10^5$ (Amps/m)
AK	k_1	Propagation constant of traveling wave
AL	L	Primary length
AM	m_1	Number of primary phases
AMU2	μ_2	Relative permeability of Region 2
AMBDA	λ_3	Relative permeability of Region 3
AN	w_c	Eq'n A-8, page 140, Ref.1.
B	2_b	Turns per coil
C	d	Secondary thickness
C2	coshαd	Half primary width
E	-	Eq'n A-7, page 140, Ref.1
EFF	η_2	Number of half-filled slots in stator winding
ETA1	-	Secondary efficiency
ETA2	-	Eq'n A-15, page 141, Ref.1
FQ	f	Eq'n A-13, page 141, Ref.1
FREQ	H(ξ)	Synchronous frequency
F( )	F	Frequency
FX	a-b	Eq'n 119, page 72, Ref.1
GAP	G(ξ,a)	Thrust
G( )	P	Airgap between primary and secondary
P	ρ'	Eq'n 118, page 72, Ref. 1
P2	ρ	Number of poles
PS	π	Secondary resistivity including edge-effect
PI	P_2	Secondary resistivity
POWER	q	3.14159
Q	s	Airgap power
S	u	Number of coils (slots) per phase belt
U	u+j	Slip
UV	ν	Eq'n A-11, page 141, Ref.1
V	$\xi_1 \xi_\sigma \xi'_\sigma$	Eq'n A-11, page 141, Ref.1
ZA,ZB,ZC	$-k_\sigma \xi'_\sigma$	Eq'n A-11, page 141, Ref.1
Z(1)		First approximation roots. Page 73, Ref. 1
Z(2),Z(3)		Wave number of driven wave
		Roots of $H(\xi) = 0$.

Listing of Yamamura Computer Program

```
C     PROGRAM COMPUTES LIN OUTPUT PARAMETERS USING YAMAMURA THEORY FOR
C     CONSTANT CURRENT EXCITATION. EDGE EFFECT INCLUDED IN CALCULATION.
C     IMODE=1 FOR VARIABLE FREQUENCY. IMODE=0 FOR VARIABLE SLIP.
C     THRUST AND POWER COMPUTED FOR ONE CORE SIDE.  MULTIPLY BY 2 FOR
C     TOTAL THRUST, POWER OF DLIM.
C     REQUIRED INPUT DATA:  AL=P X TP, W=SEC WIDTH, C=HALF CORE WIDTH
C     B=SEC THICKNESS, GAP=AIRGAP, TP=POLE PITCH, P=NO. OF POLES
C     E=NO. OF HALF FILLED SLOTS, Q=SLOTS/PHASE BELT, AN=TURNS/SLOT
C     AM=NO. PHASES, IMODE=FREQ-VERSUS-SLIP OUTPUT, PS=SEC RES X 10000000.
C     AMU2=REL PERM. OF SEC, AMU3=REL PERM OF AIR, AI1=CURRENT/CONDUCTOR
C     FREQ=MOTOR FREQUENCY. FOR VARIABLE FREQUENCY OUTPUT FORMAT, CHOOSE
C     FREQ EQUAL TO INITIAL INPUT FREQUENCY.  FQ=MOTOR SPEED/2./TP
C     MKS UNITS. LENGTH IN METERS, FORCE IN NEWTONS
      COMPLEX GAMMA1,TNH,AMBDA,UV
      COMPLEX FX21,FX22,FX31,FX32,FX11,FX42
      COMPLEX ZB,ZC,Z(9),GAMMA,E1,E2,C1,C2,S1,S2
      COMPLEX F(3),DF(3),DERF,G(3),FX1,FX2,FX3,DZ
      COMPLEX DGAMMA,AA,BB,GAMMA2
      DIMENSION T(20),FX(20),FY(20),DEL(3,20),POWER(20),EFF(20)
    1 FORMAT(1X,5HFREQ=,F5.0,1X,3HFQ=,F6.1,1X,3HI1=,F6.0,1X,3HTP=,F6.3)
    2 FORMAT(      17X,2HFX,6X,9HP(AIRGAP),4X,3HEFF)
    3 FORMAT(4X,F6.2,2X,2(1X,E10.3),1X,F6.3)
    4 FORMAT(1X,2HL=,F6.3,1X,2HB=,F6.4,1X,2HW=,F6.3,1X,2HC=,F6.3
     1,1X,4HGAP=,F6.3,1X,2HP=,F3.0,1X,2HM=,F2.0)
    5 FORMAT(1X,2HE=,F3.0,1X,2HQ=,F3.0,1X,3HP2=,F6.3,1X,2HN=,
     1F3.0,1X,5HAMU2=,F6.2,1X,5HAMU3=,F6.2)
    6 FORMAT(2X,F4.0,F7.3,2(1X,2F7.2),2X,2(1XF4.3),3I5)
    9 FORMAT(4X,1HF,3X,5HXI(1),6X,5HXI(2),10X,5HXI(3),6X,4HETA1
     1,1X,4HETA2,3X,4HIER0,1X,4HIER1,1X,4HIER2)
   40 FORMAT(1X,6E10.3)
   41 FORMAT(6F10.4)
   42 FORMAT(5F10.1,I5)
   43 FORMAT(4F10.3)
   44 FORMAT(2F10.1)
      SQT2=SQRT(2.)
      S=1.0
      PI=3.14159
      AMU=4.*PI
      N=1
    8 CONTINUE
      READ(5,41,END=99)AL,W,C,B,GAP,TP
      READ(5,42)P,E,Q,AN,AM,IMODE
      READ(5,43)PS,AMU2,AMU3,AI1
      READ(5,44)FREQ,FQ
      XMODE=IMODE
      AK=PI/TP
      GF=2.*PI*FREQ*AMU*B/PS/(B+2.*GAP)/AK/AK
      ALPHA=PI/Q/AM
      AKW1=SIN((AM*Q-E)/2.*ALPHA)*SIN(Q*ALPHA/2.)/SIN(ALPHA/2.)
      AJZ=6.*SQT2*AN*AI1*AKW1/TP/100000.
      K=1
C     NEXT COMPUTE BOLTON'S FACTORS=ETA1,ETA2
   10 S=1.-FQ/FREQ*XMODE
      GS=GF*S
      GAMMA1=AK*CSQRT(1.+(0.0,1.0)*GS)
      E2=CEXP(C*GAMMA1)
      S2=0.5*(E2-1./E2)
      C2=0.5*(E2+1./E2)
      TNH=S2/C2
      AMBDA=1./(1.+GAMMA1*TNH*TANH(AK*(W/2.-C))/AK)
      UV=AMBDA*TNH/GAMMA1/C
```

```
      U=REAL(UV)
      V=AIMAG(UV)
      ETA1=(1.-U-GS*V)/(1.-GS*V+GS*GS*U)
      ETA2=((1.-GS*V)**2+(GS*U)**2)/(1.-GS*V+GS*GS*U)
      P2=PS/ETA1
C     NEXT COMPUTE ROOTS OF F(N) USING NEWTON-RAPHSON METHOD. ZB,ZC ARE
C     FIRST APPROXIMATION ROOTS.
      A1=2.*PI*FREQ*AMU/P2
      A2=A1*B/4./AK/(GAP+B/2.)
      ZA=-AK
      ZB=(0.0,-1.0)*A2*((1.-S)-CSQRT((1.-S)**2+(0.0,1.0)*AK/A2*2.))
      ZC=(0.0,-1.0)*A2*((1.-S)+CSQRT((1.-S)**2+(0.0,1.0)*AK/A2*2.))
      Z(1)=ZA
      Z(2)=ZB
      Z(3)=ZC
   15 CONTINUE
      S=(1.-FQ/FREQ)*XMODE+S*(1.-XMODE)
      GS=GF*S
      GAMMA1=AK*CSQRT(1.+(0.0,1.0)*GS)
      E2=CEXP(C*GAMMA1)
      S2=0.5*(E2-1./E2)
      C2=0.5*(E2+1./E2)
      TNH=S2/C2
      AMBDA=1./(1.+GAMMA1*TNH*TANH(AK*(W/2.-C))/AK)
      UV=AMBDA*TNH/GAMMA1/C
      U=REAL(UV)
      V=AIMAG(UV)
      ETA1=(1.-U-GS*V)/(1.-GS*V+GS*GS*U)
      ETA2=((1.-GS*V)**2+(GS*U)**2)/(1.-GS*V+GS*GS*U)
      P2=PS/ETA1
      A1=2.*PI*FREQ*AMU/P2
      AJ1=ETA2*AJZ
      DO 25 N=1,3
      IEND=8
      IF(N.EQ.1)IEND=1
      DO 18 I=1,IEND
      ZR2=REAL(Z(2))
      ZI2=AIMAG(Z(2))
      GAMMA3=ZR2*ZR2-ZI2*ZI2-A1*ZI2*(1.-S)/AK
      GAMMA4=2.*ZR2*ZI2+A1*ZR2*(1.-S)/AK+A1
      GAMMA2=Z(N)*Z(N)
   16 GAMMA2=(GAMMA2+(0.0,1.0)*A1*(Z(N)*(1.-S)/AK+1.))
      GAMMA=CSQRT(GAMMA2)
   90 DGAMMA=(Z(N)+(0.0,1.0)*A1*(1.-S)/2./AK)/GAMMA
      E1=CEXP(GAMMA*B/2.)
      E2=CEXP(Z(N)*GAP)
      C1=0.5*(E1+1./E1)
      C2=0.5*(E2+1./E2)
      S1=0.5*(E1-1./E1)
      S2=0.5*(E2-1./E2)
      IF(N.EQ.1)GO TO 20
      AA=C1*S2+Z(N)*C1*C2*(GAP)+AMU3/AMU2*GAMMA*S1*S2*(GAP)
      BB=Z(N)*B/2.*S1*S2+AMU3/AMU2*(S1*C2+GAMMA*B/2.*C1*C2)
      DERF=AA+BB*DGAMMA
      F(N)=Z(N)*C1*S2+AMU3/AMU2*GAMMA*S1*C2
      DZ=F(N)/DERF
      ADZ=CABS(DZ)
   18 Z(N)=Z(N)-DZ
C     END OF NEWTON-RAPHSON CALCULATION.
      DEL(N,K)=-ALOG10(ADZ)
C     DEL(N,K)=PARAMETER DEFINING ROOT CONVERGENCE. DEL SHOULD BE POSI-
C     TIVE AND GREATER THAN 3 FOR CORRECT RESULTS.
   20 F(N)=Z(N)*C1*S2+AMU3/AMU2*GAMMA*S1*C2
      DF(N)=DERF
      G(N)=C1*C2+GAMMA*S1*S2/Z(N)
   25 CONTINUE
```

```
      FX1=-P*TP*G(1)/F(1)*(0.0,1.0)
      ZR2=REAL(Z(2))
      ZI2=AIMAG(Z(2))*AL
      ZI3=AIMAG(Z(3))*AL
      ZR3=REAL(Z(3))
      IF(ZI2.GT.30.)ZI2=30.
      IF(ZI3.LT.-30.)ZI3=-30.
      FX21=(1.-EXP(-ZI2)*CEXP((0.0,1.0)*(ZR2+AK)*AL))
      FX21=FX21/(Z(2)+AK)
      FX31=-(1.-EXP(ZI3)*CEXP((0.0,-1.)*(ZR3+AK)*AL))
      FX22=G(2)/(Z(2)+AK)/DF(2)
      FX32=G(3)/(Z(3)+AK)/(Z(3)+AK)/DF(3)
      FX2=FX21*FX22
      FX3=FX31*FX32
      POWER(K)=-PI*FREQ*AMU*AJ1*AJ2*REAL(FX1+FX2+FX3)*2.*C*1000.
      FX(K)=0.5*AJ2*AJ1*AMU*REAL(Z(1)*FX1+Z(2)*FX2+Z(3)*FX3)
     1*1000.*2.*C
      EFF(K)=FX(K)*2.*TP*FREQ*(1.-S)/POWER(K)
      T(K)=FREQ*XMODE+(1.-XMODE)*S
      K=K+1
   28 CONTINUE
      FREQ=(FREQ+5.)*XMODE+FREQ*(1.-XMODE)
      S=(S-.1)*(1.-XMODE)+S*XMODE
      IF(K-11)15,15,30
C     PROGRAM COMPUTES 11 DIFFERENT SLIP-FREQUENCY CASES.
   30 CONTINUE
      WRITE(6,11)(DEL(2,K),K=1,11)
      WRITE(6,11)(DEL(3,K),K=1,11)
   11 FORMAT(1X,11(1X,F4.1))
      WRITE(6,4)AL,B,W,C,GAP,P,AM
      WRITE(6,5)E,Q,PS,AN,AMU2,AMU3
      WRITE(6,1)FREQ,FQ,AI1,TP
   32 WRITE(6,2)
      DO 35 K=1,11
   35 WRITE(6,3)T(K),FX(K),POWER(K),EFF(K)
      GO TO 8
   99 STOP
      END
```